SECOND LAW ANALYSIS OF A COMMERCIAL ABSORPTION REFRIGERATION SYSTEM THAT UTILIZES AMMONIA AND WATER PAIR AS WORKING FLUID

Larissa Costa Sobral

Josegil Jorge Pereira de Araújo

Iana Mota Araújo

Larissa Menezes Santos

lari_lari_12@yahoo.com.br

josegil@ufs.br

ianamotaraujo@hotmail.com

larissa.menezes.santos@hotmail.com

Universidade Federal de Sergipe

Av. Marechal Rondon, n, 49100-000, Sergipe, São Cristóvão, Brazil

Abstract. *One alternative for the Vapor-Compression Refrigeration System (VCRS) is the Absorption Refrigeration System (ARS). Unlike VCRS, which is started by electrical energy, ARS starts with thermal energy that comes from different sources like fuel combustion, solar heating, thermal waste, etc. ARS application can be justified in places where electrical energy cost is high, remote areas that have no electrical energy nearby and cogeneration system. One ARS very commonly used is the ROBUR's chiller, model ACF60, with a refrigeration capacity of 60.500 Btu/h (5 TR) that works with the ammonia water mix as working fluid and thermal energy coming from gas fuel combustion. This system can be applied for air condition (commercial and residential) and as industrial refrigeration processes. For the second-law analysis the system was divided in 11 control volumes and 18 state points. The following are determined: exergy transfer rates, entropy production rates, exergy destruction rates. Exergetic efficiency is determined on each control volume. The environment temperature, 25 °C, was considered the temperature of the dead state. The model was implemented in the EES (Engineering Equation Solver) software. In this study it was possible to determinate the second-law efficiency for the ROBUR commercial refrigeration system and which components presented the highest irreversibilities.*

Keywords: *Modelling, Simulation, Refrigeration, Absorption, Exergy*

Proceedings of the XXXVIII Iberian Latin-American Congress on Computational Methods in Engineering P.O. Faria, R.H. Lopez, L.F.F. Miguel, W.J.S. Gomes, M. Noronha (Editores), ABMEC, Florianópolis, SC, Brazil, November 5-8, 2017.

1. INTRODUCTION

One alternative to the Vapor-Compression Refrigeration System (VCRS) is the Absorption Refrigeration System (ARS). Unlike the VCRS, which is powered by electrical energy, the ARS is driven by thermal energy that may come from different sources, such as fuel combustion, solar heating, thermal waste, etc. ARS application can be justified in places where electrical energy cost is high, remote areas that have no access to electricity, and in cogeneration systems. Compared to the VCRS, the ARS efficiency is smaller, so an exergy analysis is recommended; it will show where the largest irreversibilities are located. One ARS very commonly used is the ROBUR's chiller, model ACF60, with a refrigeration capacity of 60.500 Btu/h (5 TR), which uses an ammonia-water mixture as the working fluid. Its thermal energy input comes from gas fuel combustion. This system can be used in air-conditioning (commercial and residential) and in industrial refrigeration processes, the latter being the object of this study.

Exergy analysis of absorption refrigeration systems has been carried out in a number of previous works. Varani (2001) performed energy and exergy analyses of an absorption refrigeration water-lithium bromide system in which natural gas was used as fuel. Hugo (2004) performed a thermal-economic analysis of an absorption refrigeration water-lithium bromide system. Santos (2005) performed an exergoeconomic analysis of a cogeneration system using an engine powered by natural gas and an absorption refrigeration water-ammonia system. Pereira (2006) carried out an exergy analysis of a 5 TR experimental absorption refrigeration system powered by liquefied petroleum gas (GLP) and exhaust gases. Souza (2007) carried out an exergoeconomic analysis of single-pressure absorption refrigeration cycles. Rocha (2010) conducted a theoretical and experimental study of a series double effect absorption refrigeration water-lithium bromide system. Myat, et al (2011) conducted a second law study of an absorption water-lithium bromide chiller, in transient state, and examined the system's entropy generation. Joybari and Haghighat (2016) performed an exergy analysis of a simple effect absorption refrigeration water-lithium bromide system.

1.1 Absorption refrigeration system

Figure 1 shows the schematic representation of the ARS under analysis (Araújo, 2010). According to ROBUR®, 2017, the ammonia-water solution is boiled in the generator, and two separate flows are produced: a vapor flow with high ammonia concentration (strong solution) and a liquid flow with low ammonia concentration (weak solution). The strong solution is purified in the rectifier, increasing the ammonia concentration. Ammonia vapor at high temperature and pressure is then delivered to the condenser, where it undergoes a cooling process until the vapor is condensed. The strong solution has its pressure decreased as it passes through the restrictor and is then cooled in the tube-in-tube refrigerant heat exchanger. The second restrictor reduces the pressure of the solution to the evaporator pressure. In the evaporator, the solution is heated by water and evaporated. The cold and low-pressure solution is then heated in the tube-in-tube refrigerant heat exchanger and enters the solution-cooled absorber, where the strong solution is mixed with the high-temperature weak solution coming from the generator, which had its pressure reduced by the third restrictor. The absorption process of the ammonia in water starts inside the solution-cooled absorber. Because the absorption is an exothermic process, the solution is cooled both inside the solution cooler absorber and in a portion of the condenser coil. After the described processes, ammonia is completely absorbed into water.

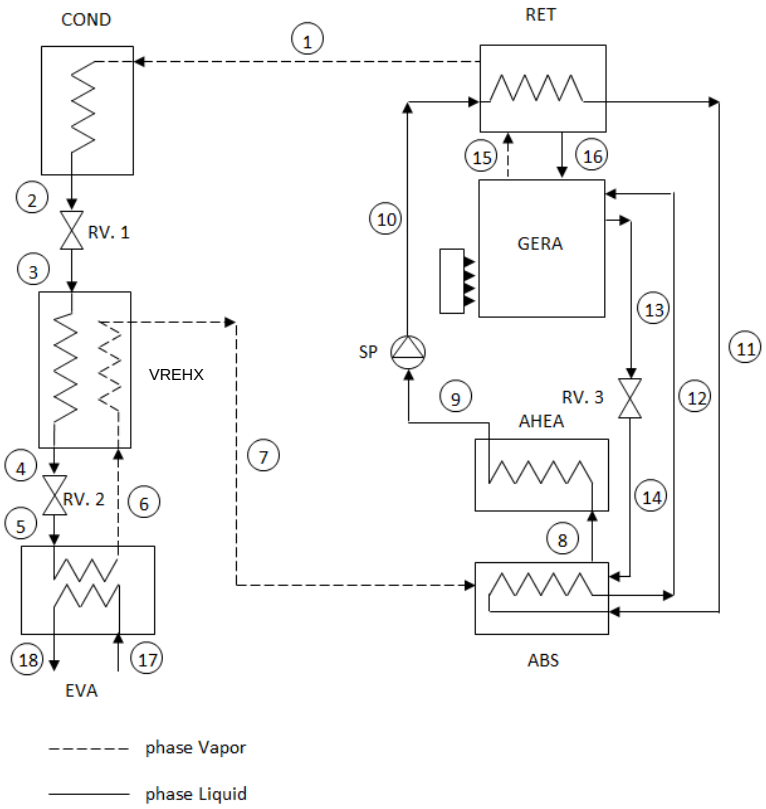

Figure 1. Schematics of the ARS, with ten control volumes and the eighteen points of state for modeling and simulation in steady state regime. (Araújo, 2010).

1.2 Thermodynamic analysis of the ARS

The study of a thermal machine may be based on energy analysis (first law of thermodynamics) or exergy analysis (second law of thermodynamics) (Moran et al., 2005). A first law study requires mass, energy and concentration balances; a second law study requires exergy and/or entropy balances. For both types of analysis, the system is divided into control volumes. State points must be defined. The properties of the state points (temperature, pressure, concentration, enthalpy, entropy, etc), the mass and work rates must be calculated, considering the adopted reference system. At last, the efficiencies of each subdivision of the system are calculated. Close examination of the results may point out possible changes and improvements to be made in the system.

1.3 Modeling and simulation

For the second-law analysis the system was divided in 11 control volumes and 18 state points. Fig. 1 shows the discretized ARS (Araújo, 2010), where the main control volumes are: generator (GERA), rectifier (RET), condenser (COND), restrictor 1 (VR1), tube-in-tube refrigerant heat exchanger (VREHX), restrictor 2 (VR2), evaporator (EVA), absorber (ABS), absorber: air heat exchanger (AHEA), solution pump (SP) and restrictor 3 (VR3). The state points are numbered from 1 to 16 for the refrigeration system and the points 17 and 18 are the entrance and exit of the water in the EVA.

The balance equations were applied using the following considerations: 1) system operates in steady state; 2) Kinetic and potential energy effects are negligible; 3) There are no pressure loss through the pipes; 4) Expansion valves are isenthalpic and 5) the flux of matter will be considered unidimensional.

The dead state temperature and pressure used to calculate entropy generation rates ($\dot{\sigma}_{ger}$), exergy production rates ($\dot{E}x_p$), exergy transfer rates ($\dot{E}x_f$) and exergy destruction rates ($\dot{E}x_d$) were considered as 25 °C and 1.013 bar, respectively. These rates were used to calculate the ratio between the exergy destruction rates and the total exergy transfer rates. The ratio between the exergy destruction rates on each control volume and the total exergy production rate was also computed. Other important performance parameters are the maximum coefficient of performance (COP_rev), the coefficient of performance (COP) (both first law efficiencies) and the exergy efficiency of the cycle (ε) (second law efficiency).

The model was implemented in the EES (Engineering Equation Solver) software, which uses the Newton-Rapson method to find the solution for the equation systems.

2 THEORETICAL FUNDAMENTS

The ARS will be studied in a first law analysis, which is based on the concept of energy conservation, and a second law analysis, based on the concept of energy quality (Çengel and Boles, 2013). Both approaches are based on the control volumes and state points as shown in Fig 1. The equations used in the analyses are presented in the following topics.

2.1 Analysis based on the concept of energy conservation

In accordance with the law of conservation of energy, mass and energy balances must be applied to the previously defined control volumes. The general form of the mass balance (Moran, et al., 2013) is:

$$\frac{dm_{cv}}{dt} = \sum_i \dot{m}_i - \sum_e \dot{m}_e \,, \tag{1}$$

in which m_{cv} is the mass in the control volume, t is the time and $\dot{m}$ is the mass flow rate. The subscripts i and e represents the inlet and exit of the control volume, respectively.

The general form of the energy balance (Moran, et al., 2013) is:

$$\frac{dE_{cv}}{dt} = \dot{Q}_{cv} - \dot{W}_{cv} + \sum_i \dot{m}_i \left(h_i + \frac{V_i^2}{2} + g z_i \right) - \sum_e \dot{m}_e \left(h_e + \frac{V_e^2}{2} + g z_e \right), \tag{2}$$

in which E_{cv} is the energy inside the control volume, $\dot{Q}_{cv}$ is the heat that enters or exits the control volume, $\dot{W}_{cv}$ is the power obtained from or given to the control volume, h is the enthalpy that enters or exits the control volume, V is the speed of the fluid that enters or exits the control volume, g is the gravity acceleration and z is the height of the system in relation to the reference state. The adopted simplifying hypotheses were: the system operates in steady state, the pressure drop along the pipes was ignored, kinetic and potential energy effects are negligible on all control volumes. The mass and energy balances were thus defined as, respectively:

$$\sum_i \dot{m}_i = \sum_e \dot{m}_e , \tag{3}$$

$$\dot{Q}_{cv} + \sum_i \dot{m}_i h_i = \dot{W}_{cv} + \sum_e \dot{m}_e h_e . \tag{4}$$

It was also assumed that all control volumes, except COND and AHEA, operate adiabatically, the expansions through the restrictors are throttling processes, and that all intensive properties are uniform across the inlet and exit areas (Moran, et al., 2013).

Since the working fluid is an ammonia-water solution, a third type of balance must be applied to the control volumes. Considering that the system operates in steady state, the ammonia concentration balance is:

$$\sum_i \dot{m}_i C_i = \sum_e \dot{m}_e C_e , \tag{5}$$

in which *C* is the ammonia concentration.

The system pressures, which are the high operating pressure of the GERA and the COND, and the low operating pressure of the EVA, ABS and AHEA, are determined according to the mathematic model proposed by Bourseau and Bugarel (1986),

$$\log(p) = A - \frac{B}{T} . \tag{6}$$

in which *p* is the pressure, *T* is the temperature and *A* and *B* are parameters determined by Eqs. (7) e (8), respectively,

$$A = 7.44 - 1.767.C + 0{,}9823.C^2 + 0.3627.C^3 , \tag{7}$$

$$B = 2013.8 - 21.557.C + 1540.9.C^2 - 194.7.C^3 , \tag{8}$$

in which *C* is the ammonia concentration.

The power supplied to the SP is determined by Eq. (9), assuming the process is isentropic, isochoric and adiabatic.

$$\dot{W}_{cv} = \left(p_{high} - p_{low}\right)\frac{v.\dot{m}}{\eta_{pump}} , \tag{9}$$

in which *v* is the specific volume of the liquid on the pump inlet, $\dot{m}$ is the mass flow rate, η_{pump} is the pump efficiency and p_{high} and p_{low} are the high and low pressures in the system, respectively.

The coefficient of performance of the Carnot refrigeration cycle is calculated by the following equation (Moran, et al.,2013):

$$COP_{Carnot} = \frac{T_C}{T_H - T_C} , \tag{10}$$

in which T_C and T_H are the temperatures of the cold and hot heat reservoirs, respectively.

The ARS coefficient of performance, COP, is the ratio of the refrigeration effect to the input required to achieve that effect (Çengel and Boles, 2013). In an absorption refrigeration

system, the refrigeration effect is the cooling provided by the EVA, $\dot{Q}_{EVA}$, and the input is the heat provided to the GERA, $\dot{Q}_{GERA}$, added to the work required by the SP, $\dot{W}_{BS}$. Mathematically:

$$COP_{ARS} = \frac{\dot{Q}_{EVA}}{\dot{Q}_{GERA} + \dot{W}_{BS}}. \tag{11}$$

The reversible coefficient of performance, COP_{rev}, is determined by the following relation (Çengel and Boles, 2013),

$$COP_{rev} = \left(1 - \frac{T_0}{T_s}\right)\left(\frac{T_L}{T_0 + T_L}\right). \tag{12}$$

in which T_0 is the environment temperature, T_s is the heat source temperature and T_L refrigerated space temperature.

Using the coefficients of performance, the cycle's efficiency, $\beta_{\max}$,(Costa, 1982), which is the ratio to the system *COP* (Eq. (11)) to the COP_{Carnot} (Eq. (10)), may be determined. This is a ratio that shows the difference between the *COP* of the studied system and COP_{Carnot}.

$$\beta_{\max} = \frac{COP}{COP_{Carnot}}. \tag{13}$$

A similar indicator of performance, $\beta_{\max,rev}$, points out the disparity between the system's actual COP and the system's reversible COP (COP_{rev}).

$$\beta_{\max,rev} = \frac{COP}{COP_{rev}}. \tag{14}$$

2.2 Analysis based on the concept of energy quality

The concept of energy quality is based on a second law analysis. To that end, an entropy balance must be carried out, so as to evaluate entropy generation in each one of the control volumes. According to Moran et al. (2013), the rate of entropy change in a control volume, $\frac{dS_{cv}}{dt}$, is expressed by the following equation:

$$\frac{dS_{cv}}{dt} = \sum_j \frac{\dot{Q}_{cv}}{T_j} + \sum_i \dot{m}_i s_i - \sum_e \dot{m}_e s_e + \dot{\sigma}_{cv}, \tag{15}$$

in which $\dot{m}_i s_i$ and $\dot{m}_e s_e$ represent, respectively, the rate of entropy transfer by mass flow at the inlet and exit of the control volume, $\frac{\dot{Q}_{cv}}{T_j}$ is the rate of entropy transfer by heat and $\dot{\sigma}_{cv}$ is the entropy generation rate due to irreversibilities that are present in the control volume.

As the present study is concerned only with steady state conditions of the ARS, the rate of entropy change in Eq. (15) becomes nil, and the equation can be reduced to:

$$\dot{\sigma}_{cv} = \sum_e \dot{m}_e s_e - \sum_i \dot{m}_i s_i - \sum_j \frac{\dot{Q}_{cv}}{T_j}. \tag{16}$$

Since entropy generation is equivalent to exergy destruction (Moran, et al.,2005), it becomes imperative to add a steady state exergy balance to the second law analysis of the system, in order to evaluate the rate of exergy destruction, $\dot{E}x_d$:

$$\dot{E}x_d = \sum_j \left(1 - \frac{T_0}{T_j}\right)\dot{Q}_{cv} - \dot{W}_{cv} + \sum_i \dot{m}_i Ex_i - \sum_e \dot{m}_e Ex_e, \tag{17}$$

in which E_x is the specific exergy of the mass flow into and out of the control volume and T_j is temperature at the boundary where heat transfer takes place. Ignoring the effects of kinetic and potential energies, specific flow exergy can be expressed by Eq. (18):

$$Ex = h - h_0 - T_0(s - s_0), \tag{18}$$

in which *h* and *s* represent specific enthalpy and specific entropy, in this order, both at the inlet and the exit of the control volume.

Alternatively, Gouy-Stodola's Theorem may be applied to determine the rate of exergy destruction. The theorem states that the rate of exergy destruction equals the product of the dead state temperature, T_0, and the rate of entropy generation (Çengel e Boles, 2013).

$$\dot{E}x_d = T_0 \dot{\sigma}_{cv}. \tag{19}$$

Bejan, et al.,1996, proposes two indexes to aid in the assessment of exergy destruction taking place in the control volumes. The first index, y_D, equals the ratio of the rate of exergy destruction in the control volume, $\dot{E}x_D$, to the total exergy supplied to the thermodynamic cycle, $\dot{E}x_{F,total}$ (Eq. 20). The second index, y_D^*, equals the ratio of the rate of exergy destruction in the control volume to the rate of exergy destruction in the entire system, $\dot{E}x_{D,total}$ (Eq. 21).

$$y_D = \frac{\dot{E}x_D}{\dot{E}x_{F,total}}, \tag{20}$$

$$y_D^* = \frac{\dot{E}x_D}{\dot{E}x_{D,total}}. \tag{21}$$

In order to assess the performance of a thermodynamic system, the exergetic efficiency – also known as second law efficiency – is calculated. It can be computed for a single control volume and for the entire system (Bejan, et al.,1996). It is defined as the ratio of the recovered exergy (output) to the supplied exergy (input) (Eq. 22).

$$\varepsilon = \frac{\dot{E}x_P}{\dot{E}x_F} = 1 - \frac{\dot{E}x_D}{\dot{E}x_F}. \tag{22}$$

The mass, energy, entropy and exergy balances are applied in accordance with the characteristics of each control volume, as shown in Fig. 1, taking into account the flow of mass into and out of the control volume, and the transfer of energy, both by heat and work.

3 MODEL IMPLEMENTATION

The mathematical model of the ARS was implemented in EES®. The results obtained from the simulation of the model provide the basis for energy and exergy analyses of the system. The following sections outline important steps of the modelling and simulation of the ARS.

3.1 Discretization of the system

The ARS was discretized as shown in Fig. 1. The energy analysis was based on fifteen control volumes; the exergy analysis was based on eleven. The same eighteen state points ware used for both analyses.

For the energy analysis, besides the control volumes coinciding with the system's components, additional control volumes were created around the following elements: the coil inside the rectifier; the inner tube in the concentric heat exchanger; the secondary refrigerant tube and the coil inside the absorber. The elements are shown in Table 1.

Table 1. Additional control volumes for energy analysis (Araújo, 2010).

Coil inside rectifier 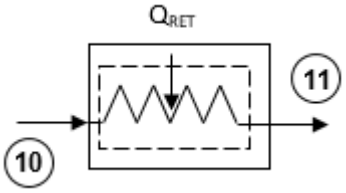	Inner tube of concentric heat exchanger 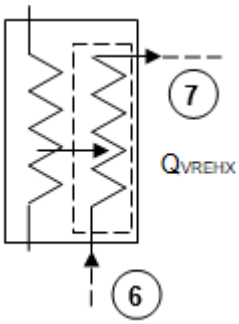
Secondary refrigerant tube 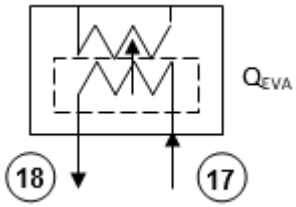	Coil inside absorber 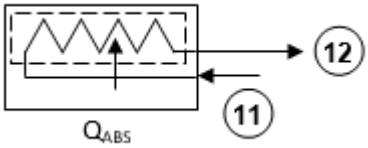

3.2 Implementation of balance equations

For each control volume, mass, energy, concentration, entropy and exergy balances were implemented. The latter was solved after the properties of all state points had been computed.

Mass, energy, entropy and exergy balances for the generator are presented in Eqs. (3) through (5), Eqs. (16) through (18), respectively.

The properties at the state points indicated in Fig 2 were computed by an external routine called NH3H2, which is based on the work of Ibrahim (1993).

With all the balances successfully implemented, a system of equations is formed, which is solved using Newton-Raphson's method.

4 RESULTS AND DISCUSSION

After defining its mathematical model, the ARS was simulated and analyzed. Properties of the 18 state points such as temperature (*T*), pressure (*p*), ammonia concentration (*C*), enthalpy (*h*), entropy (*s*) and exergy (*ex*) were determined (Fig. 2). The heat fluxes and the power supplied to the SP were also determined. The first law analysis was then performed, with the calculation of the following indicators: Carnot performance coefficient of the cycle (Eq. (10)), reversible coefficient of performance (Eq. (12)), maximum cycle's efficiency (Eq. (13)) and maximum reversible cycle's efficiency (Eq. (14)). The degree of irreversibilities ($\dot{\sigma}_{ger}$) in each control volume were thus determined and then the exergy destruction in each control volume was calculated. Finally, the indicators for the second law analysis were calculated: the exergy destruction rates y_D (Eq. (20)) and y_D^* (Eq. (21)), respectively, exergy efficiency of each control volume and exergy efficiency of the cycle.

4.1 Energy analysis of the ARS.

Initial conditions used by Araújo (2010) were used in the steady-state simulation. These values are listed on Table 2.

The pressure drop in VR1 was assumed to be 4.0 bar.

The mass flow rate of the secondary refrigeration fluid was adjusted according to the mass flow rate of the ammonia solution that flows through the EVA control volume. This was achieved by performing an energy balance for the EVA.

The initial conditions were used to obtain the data on Table 3. According to the calculated data, there are three pressure levels in the cycle: the highest pressure 13.65 bar; the intermediate pressure obtained after VR1, 9.65 bar, and the lowest cycle pressure 4.88 bar.

Table 2. Initial conditions for the ARS simulation.

Room temperature (T_{amb})	27.00 °C
Temperature at the evaporator exit (NH_3-H_2O)	5.00 °C
Temperature at the inlet of water cooler (H_2O)	12 °C
Temperature at the outlet of water cooler (H_2O)	7 °C
Quality at RET outlet	Vapor saturado
Quality at COND outlet	Líquido saturado
Quality at SP inlet	Líquido saturado
Quality at VR3 inlet	Líquido saturado
Process width (*Dx*)	0.10
Maximum ammonia concentration in the cycle	99.98%
Heat input at the generator	152.50 kJ/kg
SP's efficiency	75 %
VREHX's efficiency	50 %

The highest temperature of the cycle occurs at the generator outlet (point 13), 92.66 °C, from where to the weak solution goes to the VR3 and ABS. In this point, the state is saturated liquid with an ammonia concentration of 41.3%. The lowest ARS temperature was at point 5, inlet of EVA, 3.47 °C. It is important to note that the temperature at the evaporator exit (point 6) is 5 °C (initial condition). This difference of temperature between the inlet and outlet is due to the working fluid being a mixture, and this difference is named glide temperature, with a value of 1.47 °C in this cycle. The ARS has five different mass flow rates: 0.065 kg/s (points 1 to 7), 0.384 kg/s (points 8 to 12), 0.318 kg/s (points 13 and 14), 0.067 kg/s (point 15) e 0.001 kg/s at point 16. The lowest mass flow rate corresponds to the rectified solution exiting RET and returning to GERA. The highest enthalpy point, 1417.54 kJ/kg, is point 15, which corresponds to the ammonia-water flow rate that exits GERA and enters RET with 100% ammonia concentration and vapor quality of 1.000 (saturated vapor). Point 7 has the highest specific entropy, 4.681 kJ/kg·K. Point 15 has an ammonia concentration of 98.95%, showing that a small fraction of the solution vapor was condensed in RET, seeing as the concentration of ammonia was 100% (pure ammonia) at the rectifier outlet. In the table the vapor quality values, Q_u, are zero, indicating that the liquid is saturated; 1.000, indicating that the vapor is saturated; -0.001, indicating that the liquid is sub-cooled; 1.001, indicating that the vapor is super-saturated; and values between 0.000 and 1.000 indicate that there are two phases: liquid and vapor.

Table 3. State points with parameters obtained from the simulation.

Point	***T*** **(°C)**	***P*** **(bar)**	***m*** **(kg/s)**	***h*** **(kJ/kg)**	***s*** **(kJ/kg·K)**	***ex*** **(kJ/kg)**	***C*** (kg/kg)	***Qu***
1	37.99	13.65	0.065	1295.14	4.228	355.25	1.000	1.000
2	35.35	13.65	0.065	167.70	0.585	313.92	1.000	0.000
3	23.74	9.65	0.065	167.70	0.589	312.68	1.000	0.048
4	23.74	9.65	0.065	142.01	0.503	312.69	1.000	0.026
5	3.47	4.88	0.065	142.01	0.524	306.53	1.000	0.100
6	5.00	4.88	0.065	1272.23	4.591	224.16	1.000	0.997
7	13.46	4.88	0.065	1297.92	4.681	222.85	1.000	1.001
8	58.21	4.88	0.384	325.66	1.635	55.68	0.513	0.210
9	37.0	4.88	0.384	-73.57	0.394	26.56	0.513	0.000
10	37.16	13.65	0.384	-72.15	0.395	27.65	0.513	-0.001
11	42.87	13.65	0.384	-46.43	0.477	28.89	0.513	-0.001
12	53.65	13.65	0.384	2.36	0.629	32.41	0.513	-0.001
13	92.66	13.65	0.318	184.79	1.154	36.61	0.413	0.000
14	63.76	4.88	0.318	184.79	1.177	29.89	0.413	0.087
15	74.26	13.65	0.067	1417.54	4.600	366.48	0.989	1.000
16	74.35	13.65	0.001	97.62	0.912	43.22	0.512	0.000

Table 4 shows the heat fluxes which: enter the ARS by the GERA and EVA; exit the ARS by the COND and AHEA (the negative signal represents that the heat exits the control volume); and are internally recovered at the RET, VREHX and ABS (bolded in Table 4).

The proof that the model meets the principle of energy conservation is obtained by adding A, B, C, D and E (Table 4), which results in a value equal to zero and shows that the energy is conserved.

Table 4. Work and heat transfer in the ARS.

Component	$\dot{Q}$ **or** $\dot{W}$ **(kW)**
Heat input at GERA (**A**)	152.50
Heat recovered at RET	**9.87**
Heat output at COND (**B**)	-73.74
Heat recovered at VREHX	**1.68**
Heat input at EVA (**C**)	73.91
Heat recovered at ABS	**18.73**
Heat output at AHEA (**D**)	-153.22
Work input of solution pump (**E**)	0.55

The indicators for the first law analysis are shown in Table 5.

Table 5. Indicators for the first law analysis of the ARS.

Indicators	**Value**
Carnot coefficient of performance (COP_{Carnot})	16.14
ARS's reversible coefficient of performance ($COP_{rev.SRA}$)	5.90
ARS's coefficient of performance (COP_{SRA})	0.4829
ARS's maximum efficiency ($\beta_{max.Carnot}$) (%)	2.991
ARS's maximum reversible efficiency ($\beta_{max.rev}$) (%)	4.394

The COP_{Carnot} (Eq. (10)) was calculated considering the thermodynamic temperature of the hot fluid in the EVA (Eq. (23)) (secondary refrigeration fluid), which is given by the following equation (Bejan, et al., 1996):

$$T_h = \frac{h_{17} - h_{18}}{s_{17} - s_{18}}, \tag{23}$$

in which h is the enthalpy, 17 and 18 are the inlet and exit, respectively, of the heat exchanger at the water side (Fig. 1), s is the entropy at the same points. The COP_{Carnot} calculated was 16.14, which means this is the highest possible coefficient for the temperature of the cold reservoir, T_h, and temperature of the hot reservoir, T_{amb}. The $COP_{rev.SRA}$ (Eq. (12)) took into consideration the room temperature, the combustion gases temperature and the thermodynamic temperature of the hot fluid in EVA. The $COP_{rev.SRA}$ was equal to 5.9, as expected, lower than COP_{Carnot}. The COP_{SRA} (Eq. (11)) was equal to 0.4829, lower than 1. The $\beta_{max.Carnot}$ (Eq. (13)) was about 2.99% and $\beta_{max.rev}$ was equal to 8.18%, indicating that the value of COP_{SRA} is closer to the latter.

4.2 Exergy analysis of the ARS.

For the second law analysis, new initial conditions must be added, as the dead state temperature and the combustion gases temperature. For the dead state, it was adopted the conditions of the standard state of 25 °C for T_0 and 1.013 bar for P_0. For the combustion gases it was adopted 200 °C. In Table 6 the calculated parameters that were used for the second law analysis are shown.

From the analysis of Table 3 it is noted that the point of highest exergy is point 15, 366.48 kJ/kg, which is located at the generator outlet, with a temperature of 74.26 °C. The point with the lowest exergy is point 9, 26.56 kJ/kg, whose temperature is 37.0 °C. As expected, the further the point is from the temperature of the dead state, the greater its exergy will be.

In Table 6, the entropy generation, $\dot{\sigma}_{ger}$, the destroyed exergy, $\dot{E}x_d$, and the second law efficiency ε are show for each control volume.

Table 6 shows that the control volume with the greatest generated irreversibility is GERA, with 109.9 W/K, followed by AHEA with 34.66 W/K and COND with 7.416 W/K. The largest destruction of exergy occurs in GERA with 32.76 kW, followed by AHEA with 10.16 kW. The AHEA, which presented the second largest irreversibility, wasted 10.16 kW of exergy, ranking second amongst the largest wasters. As for the second law efficiency of the components, SP is the most efficient, using 75.29% of the energy available in this control volume. The lowest efficiency component was AHEA, using only 9.14% of the energy available, followed by ABS with 9.81%. The three pressure reducing valves have efficiency equal to zero, since these are considered to be adiabatic and isoenthalpical. The second law efficiency of the VREHX was not calculated, since it works with the hot fluid transferring heat almost always above the neutral temperature and the cold fluid receiving heat below the neutral temperature, therefore, it is not possible to accurately define the product and source of exergy (Bejan, et al., 1996). The second law efficiency of the ARS was 0.0719 (7.19 %).

Table 6. Entropy generation, exergy destruction and second law efficiency for each control volume.

Component	$\dot{\sigma}_{ger}$ **(W/K)**	$\dot{E}x_d$ **(kW)**	ε **(%)**
ABS	5.05	1.365	9.81
AHEA	34.06	10.16	9.14
SP	0.4452	0.1327	75.96
COND	7.416	2.211	18.18
EVA	4.463	1.331	75.29
GERA	109.9	32.76	52.45
RET	1.976	0.7179	39.72
VR1	0.2723	0.0812	0.00
VR2	1.351	0.4028	0.00
VR3	7.182	2.141	0.00
VREHX	0.2874	0.08569	-

Since the exergy analysis aim is to identify the components that have the greatest irreversibilities and the greatest destruction of exergy, the GERA and AHEA are chosen for further verification of the behavior of the irreversibility and exergy destroyed in these components in relation to the variation of the ambient temperature, the temperature evaporator exit and the variation of the heat supplied in the generator.

4.2.1 Analysis of environment temperature variation

The temperature of the environment in which the ARS operates was varied from 25 °C to 42 °C, maintaining the EVA water inlet temperature at 12 °C and the exit at 7 °C, the heat flow in the generator was maintained at 152.5 kW and the temperature at the EVA exit on the solution side was maintained at 5 °C.

In Figure 6 the behavior of the irreversibilities and the destruction of exergy on the AHEA and GERA can be observed. It is noted that the entropy generated in GERA decreases with the increase of the room temperature, with maximum value in the coordinate (25.0 °C, 115 W/K) and the minimum value in (42.0 °C, 75.38 W/K). This decrease is due to the reduction of the entropy change in the generator, since the heat portion remains constant (322.3 W/K). The destruction of exergy in GERA shows the same behavior with the maximum value in (25.0 °C, 34.32 kW) and the minimum in (42.0 °C, 22.48 kW). In AHEA, irreversibility has a small growth, such as the maximum value at (42 °C, 37.29 W/K) and the minimum value at (25 ° C, 33.58 W/K). The exergy destroyed in the AHEA increases with the increase of the room temperature, with the maximum value in (42 °C, 11.12 kW) and the minimum in (25 °C, 10.01 kW). This increase is caused by irreversibilities generated by AHEA.

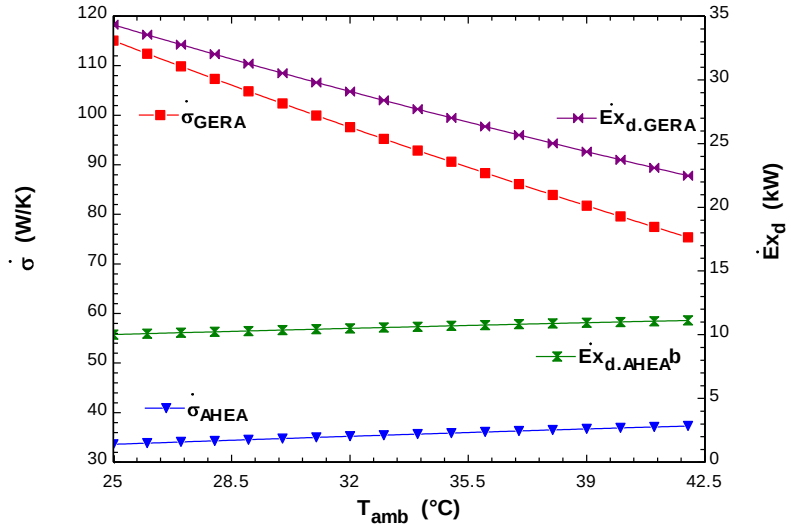

Figure 6. Influence of environment temperature on irreversibility generation and exergy destruction at ABS and GERA.

4.2.2 Analysis of evaporator outlet temperature variation

The temperature at the evaporator exit, point 6, was varied from 2.8 °C to 7 °C, maintaining the temperature of the water at the EVA inlet at 12 °C and exit at 7 °C, the heat flow in the generator was maintained at 152.5 kW and the room temperature was maintained at 27 °C.

In Figure 7 the behavior of the irreversibilities and the destruction of exergy on the AHEA and GERA can be observed. It is observed that in AHEA there is a decrease in the generation of irreversibility with the increase of temperature of point 6. The maximum generation occurs in (2.8 °C, 34.88 W/K) and the minimum in (7.0 °C ; 33.31 W/K). The exergy destruction in AHEA decreases with temperature variation, with maximum value in (2.8 °C, 10.4 KW) and minimum in (7.0 °C, 9.93 kW). In GERA there is a slight increase in irreversibilities with a minimum of (2.8 °C, 107.1 W/K) and a maximum of (7.0 °C, 112.4 W/K). The exergy destruction increases in GERA with a minimum of (2.8 °C, 31.94 kW) and a maximum of (7.0 °C, 33.54 kW).

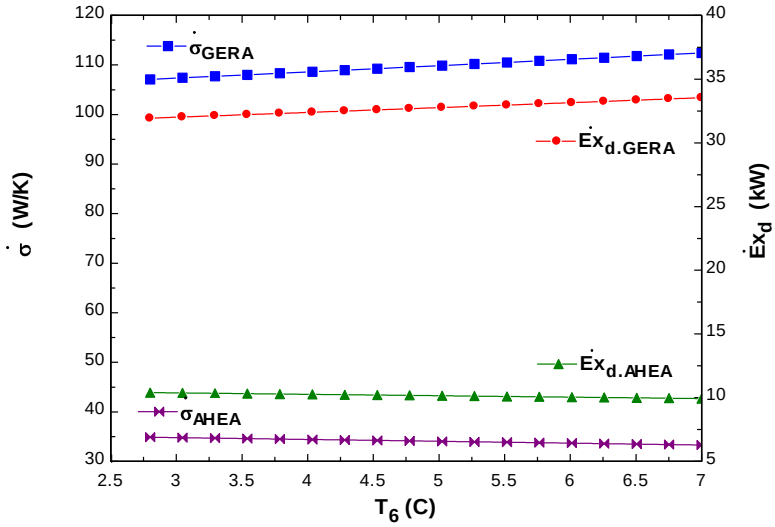

Figure 7. Varying Evaporator outlet temperature from 2.8 °C to 7.0 °C.

4.2.3 Analysis of generator heat input variation

The heat flow was varied from 140 kW to 250 kW, keeping the water inlet temperature at EVA at 12 °C and the exit at 7 °C, the temperature at the EVA exit at 5 °C and the room temperature was maintained at 27 °C.

Figure 8 shows the behavior of the irreversibilities and the destruction of exergy on the AHEA and GERA. The irreversibility in the AHEA grows with the increase of the heat flow for the GERA. The minimum occurs at (140 KW, 31.27 W/K) and the maximum at (250 kW, 55.84 W/K). The destruction of exergy in AHEA also grows when increasing the heat flow, with a minimum of (140 kW, 9.323 kW) and a maximum of (250 kW, 16.65 kW). The generation of irreversibility increases in GERA, but with a greater slope than in AHEA. The minimum occurs in (140 kW, 100.8 W/K) and the maximum in (250 kW, 180.1 W/K). The destruction of exergy in GERA also considerably increases with the increase of heat flow in GERA. The minimum value is in (140 kW, 30.08 kW) and the maximum in (250 kW, 53.71 kW).

In Figure 9 the heat flux behavior in EVA, ABS, RET, VREHX, COND and AHEA can be observed. All components had an increase in heat flow with the increase of the heat supplied in the generator. In all components the minimum value occurs for a heat flow of 140 kW and the maximum value for a heat flow of 250 kW.

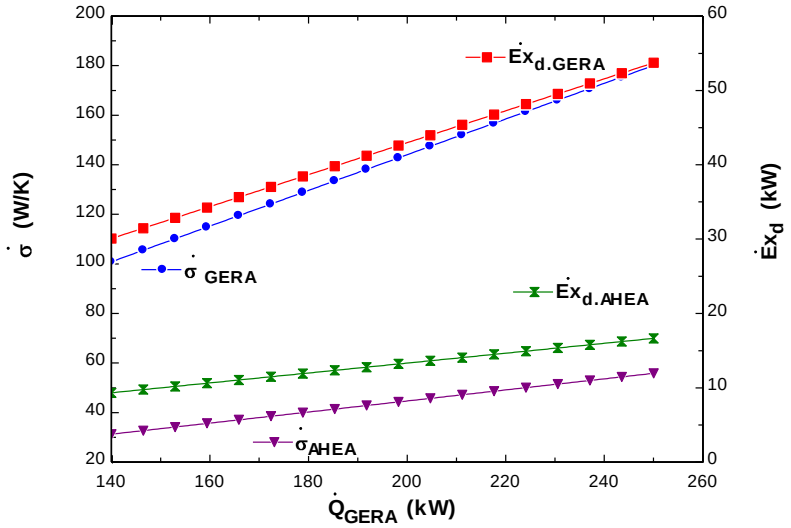

Figure 8. Varying generator heat from 140 kW to 250 kW.

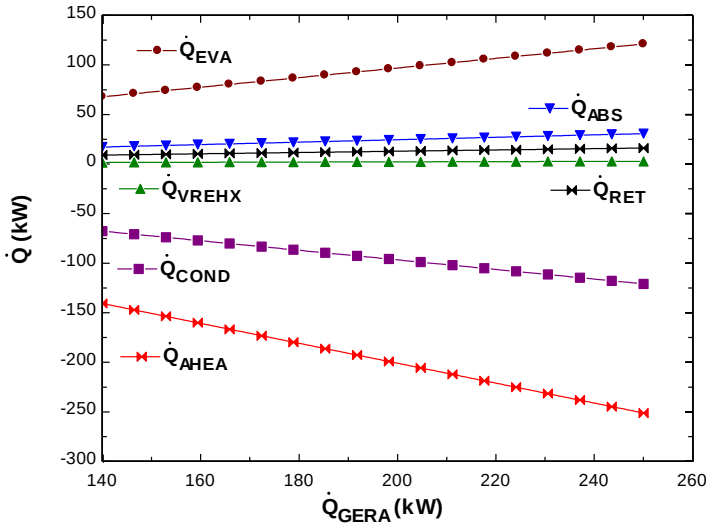

Figure 9. Influence of GERA heat input on EVA, ABS, RET, VREHX, COND and AHEA control volumes.

From the analysis of Fig. 9, it is noted that the heat fluxes in COND and AHEA have negative values, indicating that the heat is transferred out of the control volume. In COND the minimum heat flux is 67.88 kW and the maximum is equal to 120.9 kW. The heat rejected by the condenser increases due to the increase in the mass flow rate released in GERA (minimum of 0.06 kg/s and maximum of 0.107 kg/s). In AHEA there is an increase in the heat flow out of the system, in order to cool the ammonia-water solution. The minimum and maximum values for the heat flux rate in this component were 140.7 KW and 251.2 kW, respectively. In ABS, RET and VREHX the heat flow rate is small with a small variation between the minimum and maximum flow. The minimum and maximum heat flow in these components are: ABS: minimum of 17.19 kW and maximum of 30.7 kW; RET: minimum of 9.06 kW and maximum of 16.18 kW; VREHX: minimum of 1.542 kW and maximum of 2.754 kW. In the EVA there was a considerable increase of the heat flow with the variation of the heat flow in the GERA. This corresponds to an increase in the cooling capacity due to the increase in the mass flow rate of the EVA solution (minimum of 0.06 kg/s and maximum of 0.107 kg/s).

In Figure 10 the behavior of the rates of exergy destruction y_D and y_D^* can be observed. The first correlates the destruction of exergy with the source of heat exergy in the generator (Eq. (20)) and the second correlates the destruction of exergy with the total exergy destroyed (Eq. (21)). The y_D rate for AHEA increases when increasing room temperature, with a minimum value in (27 °C, 18%) and maximum in (42 °C, 19.7%). For GERA y_D decreased (maximum in (27 °C, 58.1%) and minimum in (42 °C, 39.7%)). y_D^* has the same behavior of y_D. For AHEA, the rate y_D^* has a minimum of (27 °C, 2.7%) and a maximum of (42 °C, 3.8%). For GERA the rate y_D^* presents a maximum at (27 °C, 63.8%) and a minimum at (42 °C, 51.7%).

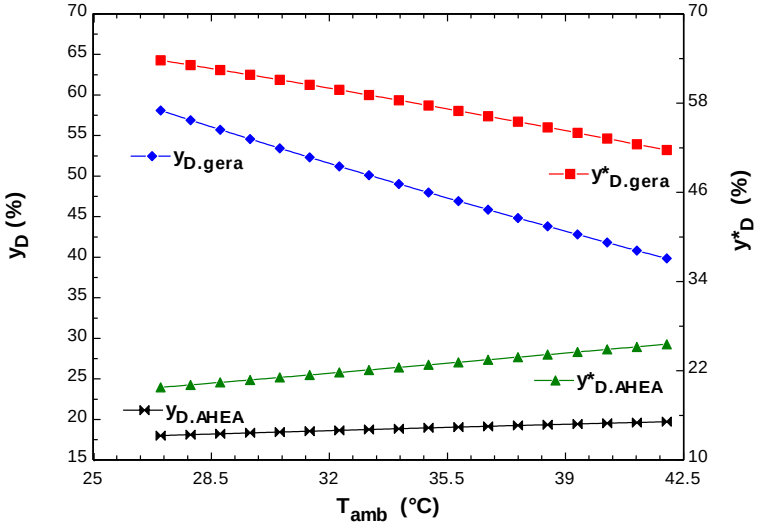

Figure 10. Behavior of exergy destruction indexes y_D e y_D^* with varying environment temperature.

In Figure 11, y_D and y_D^* are now plotted with the temperature of point 6 ranging from 2.8 °C to 7.0 °C. In this situation, y_D for AHEA decreases with the increase of T_6 with the maximum value at (2.8 °C; 18.4%) and the minimum at (7.0 °C, 17.6%). For GERA, y_D increases with T_6 with the minimum value at (2.8 °C, 56.6%) and the maximum at (7.0 °C, 59.5%). For y_D^* in AHEA this rate decreases with the increase of T_6, with a maximum value at (2.8 °C, 20.1%) and a minimum at (7.0 °C, 19.4%). For GERA, y_D^* increases with the increase of T_6, with a minimum value at (2.8 °C, 61.9%) and a maximum at (7.0 °C, 65.6%). It should be noted that the behavior of the rates is the inverse of the behavior for the case in which there is the variation of the room temperature.

Varying the heat flow rate in the GERA from 140 kW to 250 kW, the values for y_D and y_D^* remain constant, with the following values for y_D: for AHEA, 18.0%; for GERA, 58.1%. For y_D^*: for AHEA, 12.1% and for GERA: 39.1%.

4.2.4 Analysis of second law efficiencies

The second law efficiencies in the control volumes were determined, and it was analyzed which components are more efficient in harnessing the available energy. Fig. 12 shows the behavior of the second law efficiency in ABS, AHEA, SP, GERA, RET, COND control volumes when the ambient temperature ranges from 27 °C to 42 °C.

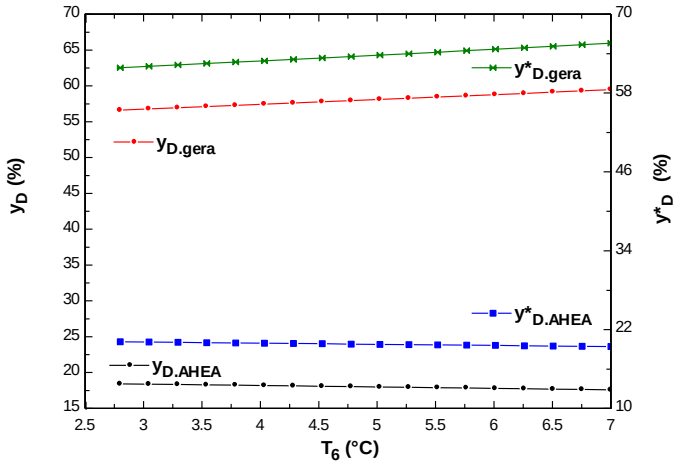

Figure 11. Behavior of exergy destruction indexes y_D e y_D^* with varying T6.

It should be noted that all control volumes have their efficiencies increased by the increase of the room temperature, but some are more sensitive to this variation than others. The solution SP and the ASP have a small improvement in efficiency, the AHEA and COND, however, are more sensitive to the room temperature variation.

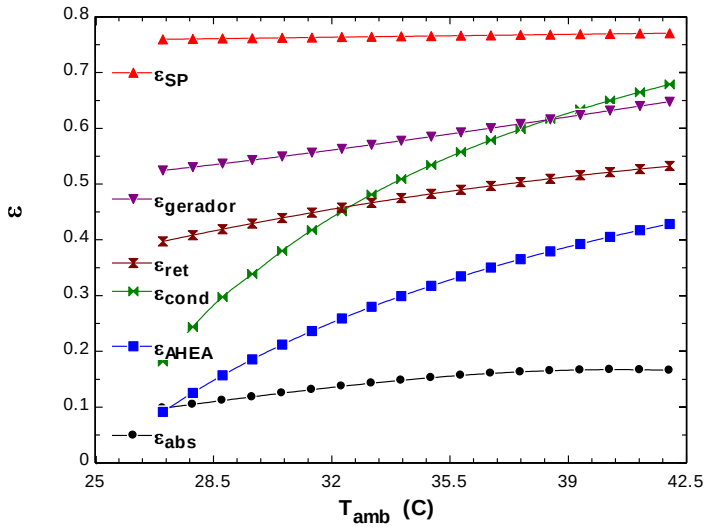

Figure 12. Influence of environment temperature on second law efficiency.

COND is the component with the greatest efficiency increase, with a minimum efficiency of 18.2% and a maximum of 67.89%. The second is AHEA, which has a minimum of 9.1% and a maximum of 42.7%. The room temperature has a low influence on the solution SP, but its average efficiency is 76.2%. The EVA second law efficiency does not change when the room temperature is changed, presenting a constant value of 75.25%.

The efficiency of the cycle decreased when increasing room temperature, with a maximum value in (27 °C, 7.2%) and a minimum in (42 °C, 4.9%). The maximum reversible efficiency of ARS increased when increasing room temperature, presenting a minimum value in (27 °C; 8.18) and a maximum in (42 °C; 11.2).

Figure 13 shows the second law efficiencies when the temperature at point 6 ranges from 2.8 °C to 7.0 °C. All control volumes had an increase in second law efficiency when increasing

the temperature, except ABS, which had a decrease in efficiency. Its maximum value occurs in (2,8 °C, 11,1%) and the minimum in (7 °C, 8.7%). It should be noted that only the evaporator has a considerable increase of efficiency with the increase of the temperature of point 6. The minimum value is 67.5% and the maximum is 84.02%. The CONDO and SP solution did not show any variation in efficiency, presenting 18.2% and 75.9%, respectively. Cycle efficiency ranged from 6.8% for a temperature of 2.8 °C to 7.5% for a temperature of 7 °C. The system's maximum reversible efficiency increased when increasing temperature of point 6 from a minimum of (27 °C, 7.75) to a maximum of (42 °C, 8.59).

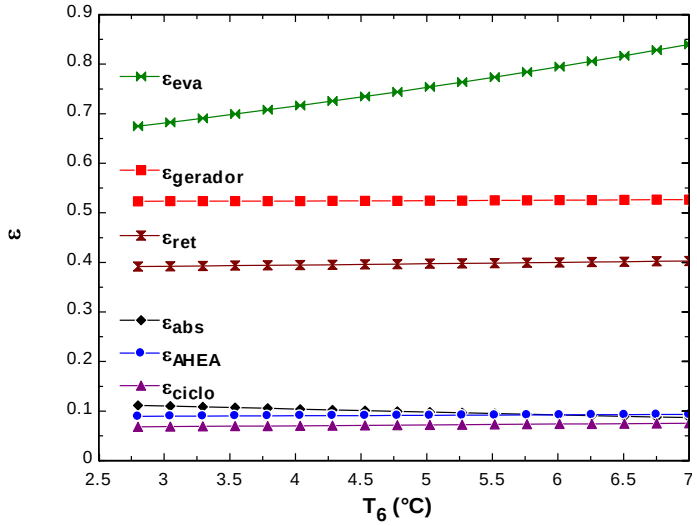

Figure 13. Influence of temperature at point 6 on second law efficiency.

5 CONCLUSION

Using the model developed for the ROBUR® ARS in steady state (implemented in EES®) and taking into account the initial conditions presented, the simulation was able to provide the properties of the 18 state points, the irreversibilities, the destroyed exergy and the second law efficiency in the 11 control volumes. It was also possible to study the behavior of irreversibilities, exergy destruction, second law efficiency, and exergy destruction rates when the ambient temperature ranged from 27 °C to 42°C, when the temperature of point 6 (evaporator exit, EVA) ranged from 2.8 °C to 7 °C and when the heat supplied in the generator ranged from 140 kW to 250 kW.

The following conclusions can be drawn from the calculated data:

- The model followed the law of energy conservation, as the sum of the incoming energies equaled the energies coming out of the ARS.
- For the first law analysis the ARS showed the following indicators: $COP_{rev}.SRA$ equals 5.90, COP_{SRA} equals 0.4829, ARS's maximum efficiency ($\beta_{max.Carnot}$) has a value of 2.99 % and ARS's maximum reversible efficiency ($\beta_{max.rev}$) has a value of 8.18.
- Point 15, at the generator outlet, had the highest specific exergy, 366.48 kJ/kg, with the temperature of 74.26 °C and entropy of 4.6 kJ/kg·K.

- The control volume with the highest exergy destruction was the generator, 32.76 kW, followed by the absorber: air heat exchanger, 10.16 kW.
- The control volume with the highest second law efficiency was the solution pump, 75.49 %, and the control volume with the lowest efficiency was the absorber: air heat exchanger, 9.14 %.
- The irreversibility generated and destruction of exergy in the absorber heat exchanger decreased with the increase of the temperature of point 6. In the generator, both the irreversibilities generated and the destruction of exergy increased with the increase of the temperature of point 6.
- When increasing the heat input at the generator, the irreversibilities and the exergy destruction increased with the increase of the heat flow in both the generator and the air heat exchanger, however the generator was more sensitive to this variation.
- The evaporator, condenser and air heat exchanger have greatly increased heat flow when increasing heat flow in the generator. In the absorber, rectifier and concentric heat exchanger the increase was less relevant.
- The exergy destruction rates, y_D and y_D^*, remained constant in relation to the variation of the heat flow in the generator, but vary with the variation of the room temperature and the temperature of point 6.
- The second law efficiency was increased in the generator, rectifier, condenser, air heat exchanger and absorber when room temperature was increased. The component that had the highest increase in efficiency caused by this variation was the condenser.
- The second law efficiency was increased in the evaporator, generator, rectifier and absorber when the temperature of point 6 was increased. The absorver heat exchanger, however, had its efficiency decreased when the temperature of point 6 was increased.
- The cycle efficiency had a slight increase when the temperature of point 6 was increased.
- The maximum reversible efficiency of the ARS had a slight increase when the temperature of point 6 was increased.

In conclusion, the model and simulation that were carried out allow the study of the refrigeration system of ROBUR®. The entry conditions may be altered, enabling several analysis of this specific cycle.

REFERENCES

Araújo, J. J. P. A, 2010. Simulação de uma unidade de refrigeração por absorção usando o par água-amônia nos regimes permanente e transiente. Tese de D.Sc., CT/UFPB, João Pessoa, PB, Brasil.

Bejan, A. Tsatsaronis, G., Moran, M., 1996. *Thermal design & optimization*. John Wiley & Sons, Inc. USA.

Bourseau, P., Bugarel, R., 1996. *Absorption-Diffusion Machines: Comparasison of the performances of NH3-H2O and NH3-NaSCN,* Int. J. of. Refrig., Vol. 9.

Çengel, Y. A., Boles, M. A., 2013. Termodinâmica. Mc, 7ª. Edição, AMGH, Porto Alegre, Brasil.

Costa, E. C., 1982. Refrigeração. 3ª. Ed., Blucher, São Paulo, Brasil.

Herold, K. E.; Radermacher, R.; Klein, S. A., 1996. Absorption chillers, heat pumps. CRC Press, Inc.

Ibrahim, O. M.; Klein, S. A., 1993. *Thermodynamic properties of ammonia-water mixtures*, ASHRAE Transactions Symposia, CH-93-21-2, pp. 1495-1502.

Joybari, M. M., Haghighat, F., 2016. *Exergy analysis of single effect absorption refrigeration systems: The heat exchange aspect, Energy Conversion and Management*, Volume 126, , Pages 799-810, ISSN 0196-8904.

Moran, M. J., Shapiro, H. N., Boettner, D. D., Bailey, M. B., 2013. Princípios de termodinâmica para engenharia, 7ª. Ed., Rio de Janeiro, LTC – Livro Técnicos e Científicos Editora S. A..

Moreira, H. L., 2004. Análise Termoeconômica de Sistemas de Refrigeração por Absorção com o Par Água-Brometo de Lítio. Tese de D.Sc., CT/UFPB, João Pessoa, PB, Brasil.

Myat, A., Thu, K., Kim, Y. D., Chakraborty, A., Chun, W. G., Ng, K. C., 2011. *A second law analysis and entropy generation minimization of an absorption chiller, Applied Thermal Engineering*, Volume 31, Issue 14, 2011, Pages 2405-2413, ISSN 1359-4311.

Pereira, M. V. A., 2006. Análise exergética experimental de uma unidade de refrigeração por absorção de 5 TR movida a gás liquefeito de petróleo (GLP) e/ou gases de exaustão. Dissertação de M.Sc., UFPB, João Pessoa, PB, Brasil.

ROBUR Site (20/08/2017), http://www.roburcorp.com/downloads/1265/290/D-LBR323_rev.N_17MCMSDC013_ACF-USA_CSA-60Hz_en.pdf.

Rocha, M. A., 2010. Estudo teórico - experimental de um sistema de refrigeração por absorção de duplo efeito em série usando o par água - brometo de lítio. Dissertação de M.Sc., UFPB, João Pessoa, PB, Brasil.

Santos, C. M. S., 2005. Análise exergoeconômica de uma unidade de cogeração a gás natural com refrigeração por absorção. Dissertação de M.Sc., UFPB, João Pessoa, PB, Brasil.

Sousa, W. L., 2007. Análise teórica exergo econômica de ciclos de refrigeração por absorção de única pressão. Tese de D.Sc., CT/UFPB, João Pessoa, PB, Brasil.

Varani, C. M. R., 2001. Avaliação Energética e Exergética de uma Unidade de Refrigeração por Absorção Àgua/Brometo de Lítio Utilizando Gás Natural, Tese D.Sc., CPGEM/CT/UFPB, João Pessoa, PB, Brasil.